JMEPEG (2011) 20:468–475
DOI: 10.1007/s11665-010-9702-5

1059-9495/$19.00

Thermal Memory Degradation in a Cu-Zn-Al Shape Memory Alloy During Thermal Cycling with Free Air Cooling

L.G. Bujoreanu, N.M. Lohan, B. Pricop, and N. Cimpoeşu

(Submitted December 27, 2009; in revised form May 20, 2010)

A fragment of a Cu-15Zn-6Al (mass%) shape memory alloy (SMA), in hot rolled-water quenched condition, was subjected to thermal cycling performed by means of a differential scanning calorimetry (DSC) device. Each cycle comprised controlled heating, isothermal maintaining, and free air-cooling, repeated three times, up to maximum temperatures increased by every 10 K, between 450 and 490 K, aiming to reproduce actual functioning conditions of a SM electrical actuator with uncontrolled cooling. Both the endothermic peaks, associated with thermally induced reversion of martensite to austenite, and their derivatives were analyzed in terms of critical transformation temperatures and specific enthalpy absorptions and in terms of transformation rates, respectively, with the aim of revealing their variational tendencies with increasing heating temperature to the maximum. The progressive decay of reverse martensitic transformation was associated with the reciprocal blocking of differentially oriented populations of stabilized lath-martensite needles, observed by scanning electron microscopy.

Keywords differential scanning calorimetry, metallography, reverse martensitic transformation, stabilization, thermal cycling

1. Introduction

Cu-Zn-Al-based shape memory alloys (SMAs) have been investigated for the last almost four decades (Ref 1) during which they became commercially available (Ref 2) due to their relatively low cost, good electrical and thermal conductivities, high ductility, and resistance to intergranular fracture (Ref 3). Consequently, some industrial applications have been developed such as hydraulic and electric couplings (Ref 4) or high work-output thermal actuators (Ref 5, 6) used for fire protection (Ref 7) or for temperature monitoring in freezing chambers (Ref 8). Considering their highly attractive potential for applications, various projects concerning electric actuators (Ref 9) low thermal-expansion elements (Invar-type effect) (Ref 10), heat engines (Ref 11), high temperature applications (Ref 12), anti-seismic dampers (Ref 13), or even "mechanical refrigerators" (based on a strong elastocaloric effect) (Ref 14) were introduced. Concomitantly, special design principles (Ref 15) were developed for Cu-Zn-Al actuators (Ref 16), and although most of them comprised polycrystalline active elements under wire spring form (Ref 17) single crystals were also proposed as a potential alternative (Ref 18).

In spite of the promising development perspectives as constrained-recovery or work-generating applications, the use Cu-Zn-Al SMAs has been hindered by a series of drawbacks caused by metallurgical processing (Ref 19, 20), training (Ref 21), and cycling (Ref 22). In particular, thermal fatigue was reported to be the primary cause for the change of critical temperatures for reverse martensitic transformation accompanied by the alteration of thermal hysteresis and the formation of oriented equilibrium phases (Ref 23-25), as an effect of diffusion. As a result, the degradation of shape memory effect (SME) was noticed in Cu-Zn-Al which was ascribed to the high temperature stabilization of martensite (Ref 26) or to the formation of rhombohedral martensite plates which were irreversibly broken up by twinning (Ref 27).

In the case of most of the actual electric actuators normal functioning involves being periodically subjected to controlled heating, accompanied by reverse martensitic transformation which triggers work-generating SME, followed by free-air cooling after electric current is cut off in such a way that direct martensitic transformation occurs and the alloy recovers its "cold shape" by two-way shape memory effect (TWSME) (Ref 28). Considering that, under such cycling conditions, the direct and reverse martensitic transformations occur in different ways and often even the thermal cycling range is varied, a gradual depreciation of thermal memory behavior is expected to occur. Therefore, this article aims to monitor the evolution of a Cu-Zn-Al SMA during thermal cycling comprising controlled heating and free-air cooling and to correlate this evolution with microstructure changes.

2. Experimental Procedure

A SMA with nominal chemical composition Cu-15Zn-6Al (mass%) was cast, hot pressed, and hot rolled (at 1020 K) to plates of 1.2×10^{-3} m thickness. The plates were instantly

L.G. Bujoreanu, N.M. Lohan, B. Pricop, and **N. Cimpoeşu**, The "Gh. Asachi" Technical University from Iaşi, Bd. D. Mangeron, 61A, 700050 Iaşi, Romania. Contact e-mail: lgbujor@tuiasi.ro.

water quenched when leaving the rolling cylinders, which were pre-heated to 670 K, to reduce premature thermal losses. This thermomechanical treatment aimed to obtain thermally induced martensite concomitantly with thickness reduction. From such a plate, lamellas were cut with the final dimensions $1.2 \times 2 \times 50 \times 10^{-3}$ m, and from such a lamella, a fragment of 57.3 mg was cut and, after careful mechanical removal of any marks of superficial corrosion under water cooling, it was subjected to five series of three thermal cycles up to five temperatures, increased by every 10 K between 450 and 490 K, for each cycle. For this purpose, a NETZSCH differential scanning calorimeter type DSC 200 F3 Maya was used, with sensitivity: <1 μW, temperature accuracy: 0.1 K and enthalpy accuracy—generally $<1\%$. The device was calibrated with Bi, In, Sn, and Zn standards. Each of the five consecutive series of three thermal cycles was performed up to a constant maximum temperature. The first three cycles were applied up to 450 K, the second three cycles up to 460 K, and so on until reaching 490 K in the fifth series. Each thermal cycle comprised: (i) heating, with 1.67×10^{-1} K s^{-1}; (ii) isothermal maintaining for 180 s; and (iii) cooling to 300 K with a cooling rate of 8.33×10^{-2} K s^{-1}. After each series of thermal cycling, maximum temperature was increased by 10 K, and a new series was applied without removing the specimen from the crucible. The measurements were performed under Ar-protective atmosphere using corresponding correction to 570 K. Since no cooling stage was attached to the DSC device, it was able to provide a controlled cooling rate only very briefly at the beginning of cooling. Subsequently actual free air-cooling at gradually decreasing rate occurred during a period calculated by the DSC Proteus software in order to reach 300 K at a cooling rate of 8.33×10^{-2} K s^{-1}. However, actual cooling rate in free air was variable and actual temperature for the end of cooling was about 360 K. It was figured up that such cycling conditions are closer to the actual functioning of an electric actuator.

After thermal cycling was complete, the specimen was removed from DSC and embedded into BAK-B Black Phenolic Powder by means of a METKON mounting press type Metapress-M. The encapsulation cycle comprised heating to 460 K, maintaining for 390 s, and cooling to 315 K. As will be shown later, this regime does not alter the thermal history of the specimen.

After appropriate etching (Ref 25), the specimen was analyzed in polarized light, by optical microscopy, on a LEICA line comprising Aristomet light microscope and Orthomat E exponometer and by scanning electron microscopy on a SEM—VEGA II LSH TESCAN microscope, coupled with an EDX—QUANTAX QX2 ROENTEC detector. The absence of any noticeable effects of the diffusion-controlled phenomena that might occur during post hot-rolling and water quenching was ascertained by energy dispersive x-ray spectroscopy (EDX) mapping. Since no concentration gradients of Cu, Zn, and Al atoms were noticeable, it has been assumed that no diffusion-controlled phases such as bainite or α-phase were formed in initial state, after hot rolling and water quenching.

3. Experimental Results and Discussion

The DSC charts illustrating the calorimetric evolution of the specimen during the heating stages of the five consecutive series of three thermal cycles, as well as of a new series performed on the cycled specimen, are shown in Fig. 1. It is noticeable that an endothermic peak occurs during first heating, in Fig. 1(a), suggesting that the specimen in initial state contains a large amount of thermally induced martensite, which reversibly transforms to parent phase (austenite) (Ref 29). According to data evaluation results given by Proteus, reverse martensitic transformation occurs during first heating at A_s = 393.3 K, reaches maximum transformation rate and 50% of transformed phase at A_{50} = 397.8 K, and ends at A_f = 403.7 K. During thermal cycling, the peaks are changed in two manners: (i) they tend to move to higher temperatures and to increase in intensity during the first cycling series and (ii) they tend to move to lower temperatures and to become less intense, up to total extinction, during second to fifth cycling series. These observations are confirmed by the values listed in Table 1. Both the positions and intensities of the peaks, at the end of a cycling series, are fairly reproduced and the beginning of the subsequent one and this is valid also in Fig. 1(f) which reproduces cycle 3 from Fig. 1(e). After four cycling series, from Fig. 1(a)-(d), A_{50} decreased with 1.1 K and specific enthalpy decreased with more than 80%. Moreover, during the last cycling series, performed up to 490 K, the peak disappeared completely, suggesting that martensite reversion no longer occurred so that total thermal memory degradation has been accomplished. Actually, the lack of any thermal activity during heating to 490 K proves that no solid phase transition occurs in this interval and, for this reason, the temperature of 460 K, applied during encapsulation process did not alter the specimen's structure obtained after five series of thermal cycling. Two main causes could be the origin of this marked degradation of thermal memory caused by thermal cycling: (i) the lack of thermally induced martensite;and (ii) the formation of stabilized martensite.

In order to evaluate the influence that thermal cycling has on the transformation rate, the derivatives of the heat flow variation charts, during the five cycling series, are illustrated in Fig. 2. The maxima and the minima of the heat flow rate correspond to the inflection points of the DSC charts which give the average transformation rates in the first and the second halves of each reverse transformation process, respectively (Ref 30). The average rate at the beginning of martensite reversion, until 50% of the process is complete, has a negative sense while that at the end has a positive sense. According to some authors, the inflection points of the second half of the process can be considered as best measure for A_f temperatures (Ref 31) while others disregard their importance in calorimetric analysis (Ref 32). However, the position of the inflection points and the values of corresponding average transformation rates give a good insight on the symmetry and the kinetics of the transformation process, respectively. Thus, by analyzing the heat flow rate variations with temperature from Fig. 2, two tendencies are noticeable: (i) during the first cycling series the process is shifted to higher temperatures and becomes faster in its second half; (ii) during second-to-fifth cycling series, the process is slightly shifted to lower temperatures, becomes slower and slower with increasing maximum heating temperature but remains faster in its second half. These observations are confirmed by the transformation rate data, comprising the temperatures of inflection points and the values of heat flow rate, listed in Table 1: in all cases, reverse martensitic transformation ended with a higher absolute rate than it started. After four cycling series, the temperatures of the inflection

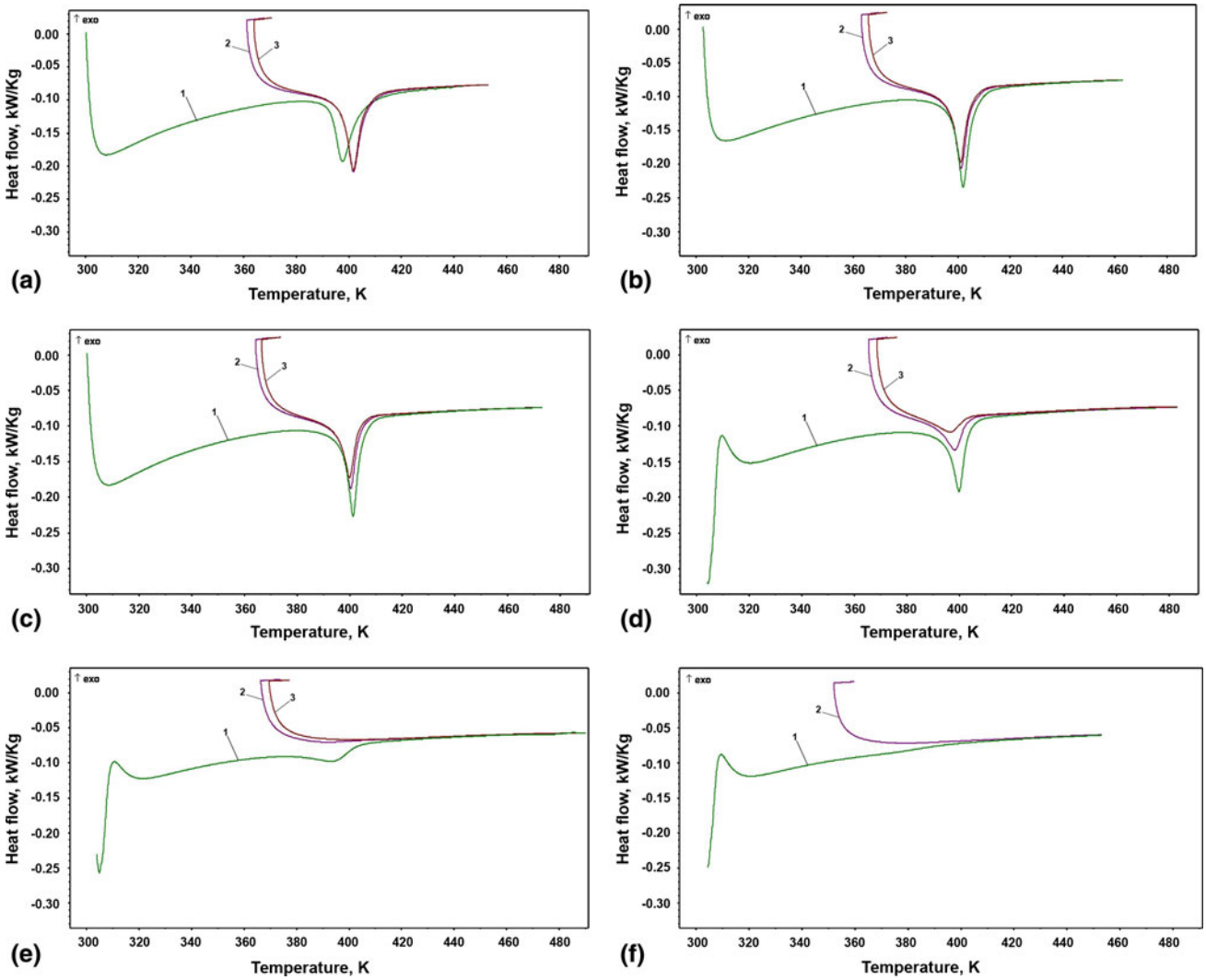

Fig. 1 DSC charts of the heating stages recorded during the consecutive thermal cycling, comprising controlled heating up to different temperatures and free air cooling, of a single fragment of hot rolled-water quenched Cu-15Zn-6Al (mass%) SMA: (a) three cycles up to 450 K; (b) three cycles up to 460 K; (c) three cycles up to 470 K; (d) three cycles up to 480 K; (e) three cycles up to 490 K; and (f) two cycles up to 450 K

points decreased with 2.6 K for the beginning of martensite reversion and with 1 K for the end, while the absolute values of the transformation rates decreased more than 12 times for the beginning and almost four times at the end of martensite reversion. These results are rather opposite to those recently reported for Cu-Zn-Al single crystals where martensite seemed to retransform faster at the beginning of transformation and not at the end (Ref 32).

As previously mentioned, the largest parts of the cooling stages were performed with free-air cooling during thermal cycling. Figure 3(a)-(e) give an insight on temperature variation with time, while Fig. 3(f) displays the evolution of minimum temperatures with maximum cycling temperatures, during each cycling series. The characteristic points on the diagrams designate the initial and the final moments of the heating stage in cycle j as $h_{j\mathrm{i}}$ and $h_{j\mathrm{f}}$, respectively while the corresponding moments of the cooling stage are $c_{j\mathrm{i}}$ and $c_{j\mathrm{f}}$, respectively. Therefore, the minimum temperature at the end of the cooling stage of cycle j corresponds to initial temperature of the heating stage in cycle $(j + 1)$, $c_{j\mathrm{f}} = h_{(j+1)\mathrm{i}}$. As noticeable from Fig. 3(f) within each series, there are two different minimum temperatures which tend to increase linearly, with increasing maximum cycling temperature. Considering the that initial structure of the specimen is martensitic, during first controlled heating, the reversion to parent phase (austenite) occurred, accompanied by the first endothermic peak, as seen from Fig. 1(a). During cooling, even if the cooling rate was variable, direct martensitic transformation occurred in such a way that thermally induced martensite formed again in the first cycling series. However, with increasing maximum temperature with 10 K in every next cycling series, Fig. 1 showed that reverse martensitic transformation became less and less intense since specific enthalpy became lower and lower. When considering this variation tendency, one should take into account that the critical temperatures for this alloy, determined on the electrical resistance versus temperature curve, have been $M_\mathrm{f} = 350$ K, $M_\mathrm{s} = 381$ K, $A_\mathrm{s} = 378$ K, and $A_\mathrm{f} = 404$ K (Ref 23), and that these values are lower than those of A_s and A_f, determined by DSC, due to the delay of the calorimetric signal (Ref 32). Therefore, considering that last cooling was performed down to

Table 1 Summary of the data determined from Fig. 1 and 2

					Heat flow rate (derivate)							
					Maximum increase		Maximum decrease				*dT*/*dt*	
Cycle No.	A_s, K	A_{50}, K	A_f, K	$\Delta H/m$, kJ/kg	*T*, K	$d(W/m)/dt$, 1.6×10^{-2} kW/kg s	*T*, K	$d(W/m)/dt$, 1.6×10^{-2} kW/kg s	Maximum temperature, K	Isothermal, s	Heating, K s^{-1}	Cooling K s^{-1}
1	393.3	397.8	403.7	−4.734	395.6	−0.235	399.8	0.160	450	180	1.67×10^{-1}	8.33×10^{-2}
2	398.1	402.1	406.4	−4.682	400.6	−0.246	403.7	0.269				
3	397.6	401.9	406.2	−5.843	400.6	−0.244	403.5	0.276				
1	398.2	402.2	406.4	−5.292	400.8	−0.302	403.6	0.353	460	180	1.67×10^{-1}	8.33×10^{-2}
2	397.5	401.3	405.5	−4.948	400.2	−0.248	402.8	0.302				
3	397.4	401.3	405.2	−4.469	400.0	−0.228	402.6	0.286				
1	397.9	401.4	404.7	−4.553	400.5	−0.312	402.6	0.402	470	180	1.67×10^{-1}	8.33×10^{-2}
2	397.3	400.5	403.7	−3.002	399.3	−0.214	401.7	0.288				
3	396.8	400.0	403.2	−2.502	398.9	−0.166	401.5	0.240				
1	395.7	400.0	403.7	−4.015	398.9	−0.191	401.3	0.303	480	180	1.67×10^{-1}	8.33×10^{-2}
2	393.4	398.4	402.8	−1.865	396.4	−0.0536	400.5	0.11				
3	391.6	396.7	402.7	−0.8001	393	−0.019	399.8	0.041				
1	389.1	393.4	402.7	−0.4958	0	0	398.7	0.0324	490	180	1.67×10^{-1}	8.33×10^{-2}
2	…	…	…	…	…	…	…	…				
3	…	…	…	…	…	…	…	…				

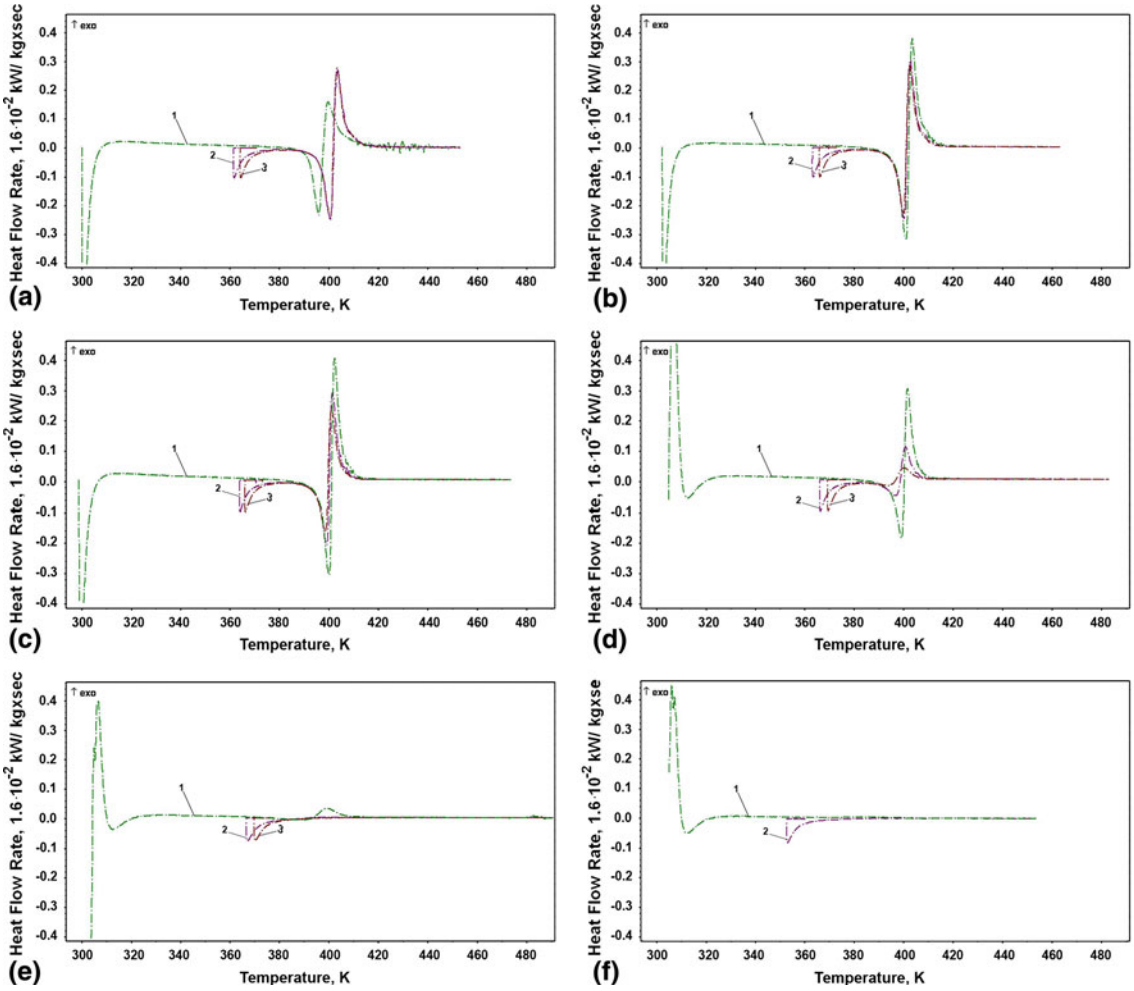

Fig. 2 Variations of the heat flow rates during the consecutive thermal cycling, corresponding to the derivatives of Fig. 1: (a) three cycles up to 450 K; (b) three cycles up to 460 K; (c) three cycles up to 470 K; (d) three cycles up to 480 K; (e) three cycles up to 490 K; and (f) two cycles up to 450 K

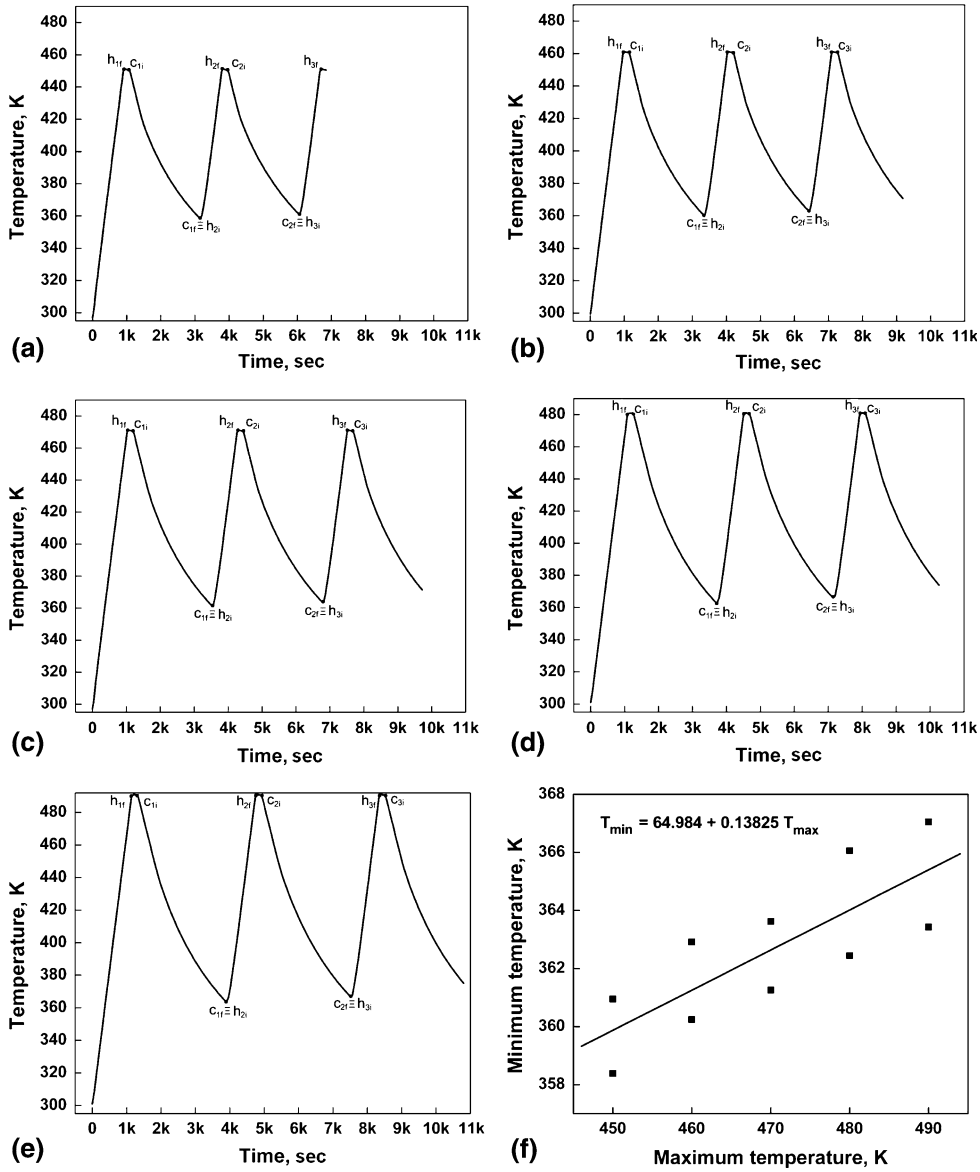

Fig. 3 Variations of specimen temperature during the consecutive thermal cycling, corresponding to Fig. 1: (a) three cycles up to 450 K; (b) three cycles up to 460 K; (c) three cycles up to 470 K; (d) three cycles up to 480 K; (e) three cycles up to 490 K; and (f) variation of minimum temperatures with maximum cycling temperatures, during the five thermal cycling series

367 K, as seen in Fig. 3(f), it is presumable that direct martensitic transformation was already triggered, since M_s = 381 K, and at least a low amount of thermally induced martensite has formed. Therefore, the total lack of thermally induced martensite cannot be considered as the cause for the disappearance of any martensite reversion on heating in Fig. 1(f). This leaves the formation of stabilized martensite as the single potential cause of thermal memory degradation. Moreover, from one series of three cycles to the subsequent one, the minimum temperature which was reached during cooling has gradually increased. This means that an increasingly amount of martensite did not form during forward (direct) martensitic transformation. In other words, an increasing amount of retained austenite was simply cooled down to the temperature of the points c_{jf} and heated up to the maximum temperature h_{jf} of the respective series, thus propitiating the stabilization of martensite.

In order to corroborate martensite reversion rate with temperature variation rate, Fig. 4(a)-(e) illustrates the derivatives of the corresponding diagrams from Fig. 3(a)-(e), respectively, determined with ORIGIN software, while Fig. 4(f) shows the dependence of minimum cooling rates (in absolute values) on maximum applied heating temperatures. By means of ORIGIN, the abscissas of the characteristic points from Fig. 3(a)-(e), were determined and marked on the same positions on Fig. 4(a)-(e), respectively. The maxima on the curves correspond to the heating rate 1.67×10^{-1} K s^{-1}, the sharp minima correspond to the very briefly applied cooling rate, 8.33×10^{-2} K s^{-1}, and the short plateaus at zero value of temperature variation rate correspond to points c_{ji} which mark the beginning of cooling. ORIGIN was used, as well, to determine minimum cooling rates reached at the end of free-air cooling stages. It is noticeable that, these values, which are illustrated in Fig. 4(f) tend to increase linearly (in absolute

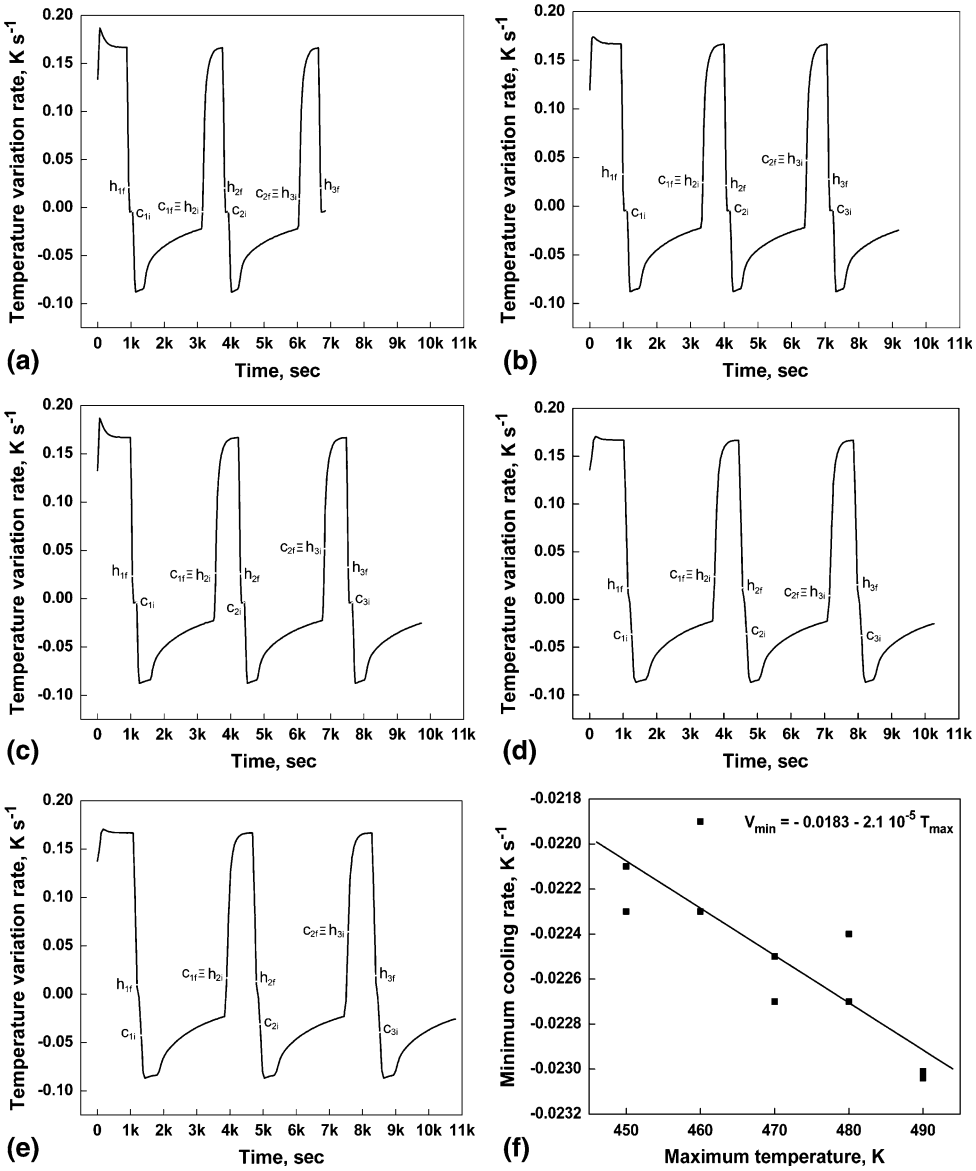

Fig. 4 Evolution of temperature variation rate during the consecutive thermal cycling, corresponding to the derivatives of Fig. 3: (a) three cycles up to 450 K; (b) three cycles up to 460 K; (c) three cycles up to 470 K; (d) three cycles up to 480 K; (e) three cycles up to 490 K; and (f) minimum values of temperature variation rates vs. maximum cycling temperatures

value), between 2.21 and 2.27×10^{-2} K s^{-1}, with increasing maximum applied temperature on heating.

The above mentioned results suggest that thermally induced martensite was formed, from retransformed austenite during free air cooling, at temperature variation rates which decreased from 8.33×10^{-2} K s^{-1} firstly to 2.21×10^{-2} K s^{-1} and then, with increasing maximum temperature applied on heating, to 2.27×10^{-2} K s^{-1}. The gradual increase of maximum temperature on heating, on one hand, and the progressive raise of temperature and cooling rate at the end of free-air cooling, on the other hand, are expected to cause microstructural changes of thermally induced martensite such as inducing its gradual stabilization and finally to fully preventing its reversion to austenite, on heating.

These changes can be emphasized starting from the typical microstructure of the specimen in initial state, shown in Fig. 5 by means of an optical micrograph in polarized light. The microstructure reveals thermally induced martensite with large primary martensite plates displaying typical diamond structure (Ref 33) and smaller secondary martensite plates with marked surface relief, in the upper left corner of the micrograph. As an effect of large cooling rate caused by water quenching, some of the primary plates display zigzag morphology (Ref 34) but even in this case, the global aspect of the plates, with twin-related martensite variants, stacking fault marks aligned along the plates and diamond-like structure, is characteristic to internally faulted thermoelastic martensite currently observed in Cu-Zn-Al SMAs (Ref 35).

After thermal cycling, as shown in Fig. 6, all the above mentioned features are no longer noticeable since the general aspect of martensite has changed. Figure 6(a) shows that martensite does no longer occur as plates but rather as needles, which are shorter and thinner, being characteristic to lath-martensite. The detail from Fig. 6(b) shows two populations of

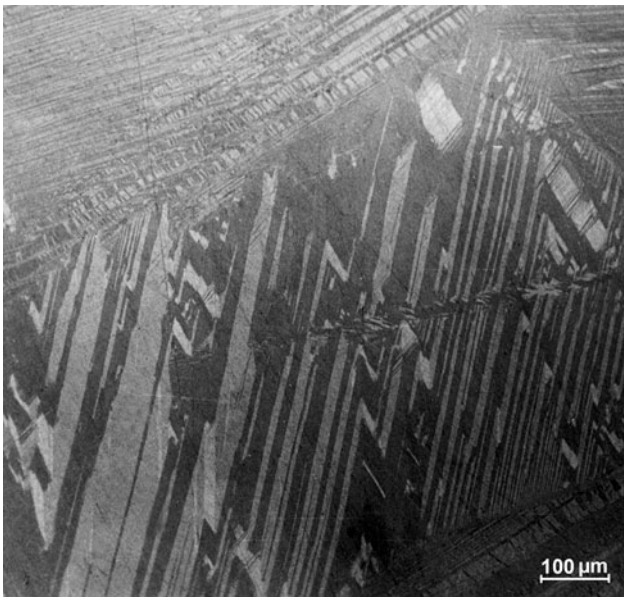

Fig. 5 Typical optical micrograph, in polarized light, of hot rolled-water quenched Cu-15Zn-6Al (mass%) SMA specimen in initial state, revealing primary and secondary plates of thermally induced martensite

differently oriented lath-martensite needles which block one another. No martensite plate variants and no relief are noticeable which could be associated with the thermoelastic accommodation of martensite or with the coherency between martensite and austenite, which would enhance the occurrence of SME.

At this point of the discussion, considering that heating temperature exceeded 450 K, one could invoke the potential occurrence of diffusion processes as another presumptive cause of thermal memory degradation. These processes could easily lead to the transitory formation of α_1 bainite (Ref 36) or to the precipitation of equilibrium α-phase. The former has diffusion-controlled growth, and, therefore, hinders transformation reversibility while the latter requires the eviction of Zn and Al atoms, from the regions occupied by Cu-rich α-phase crystallites to the matrix, thus increasing Zn and Al concentration and decreasing to much transformation temperatures of the matrix. However, one should have in mind that transitory bainite formed only after long isothermal aging, before transforming to equilibrium α-phase. Moreover, it has been shown that bainite formation during continuous heating is associated with a flat endothermic peak on DTA (Ref 37) or DSC charts (Ref 25) while α-phase precipitation was accompanied by an exothermic peak (Ref 29), which was definitely not the case in this study. Even assuming that these diffusion-controlled processes occurred, they were not intense enough to be noticeable either by DSC measurements or by EDX mapping.

4. Summary and Conclusions

A hot-rolled water-quenched Cu-15Zn-6Al (mass%) SMA, with self-accommodated thermoelastic martensite structure, experienced cyclic reversion to turn into austenite during five series of consecutive thermal cycling, comprising controlled

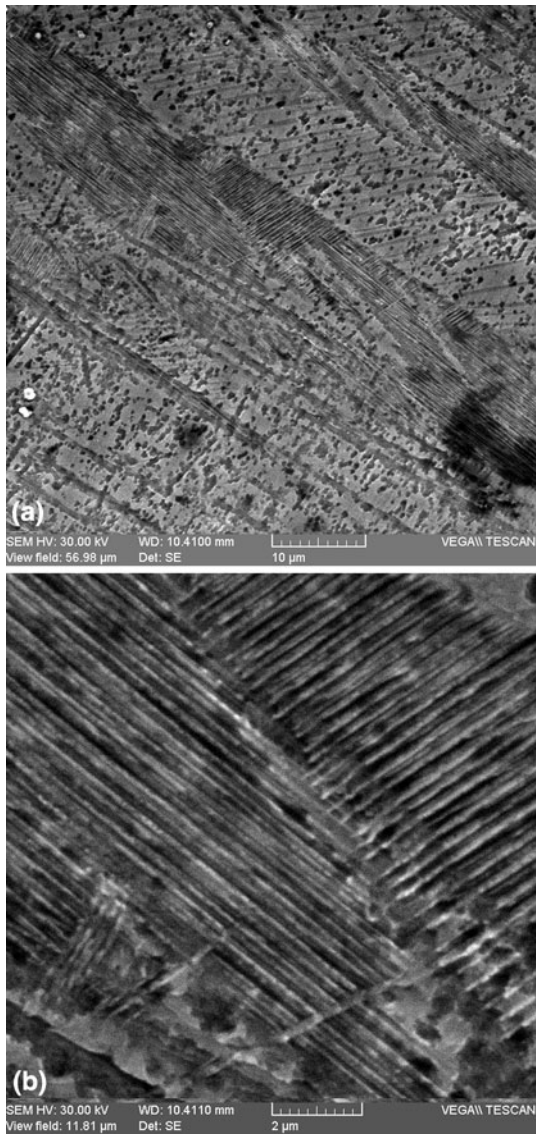

Fig. 6 SEM micrographs of Cu-15Zn-6Al (mass%) SMA specimen after the thermal cycling applied in Fig. 1: (a) general aspect; (b) detail of the intersection of stabilized lath-martensite needles

heating up to five temperatures increased by every 10 K between 450 and 490 K, under isothermal maintaining and free-air cooling. During cycling, with the increase of maximum heating temperature, the end of free-air cooling occurred at progressively higher temperatures, between 358 and 367 K and at slightly higher absolute cooling rates, between 2.21×10^{-2} and 2.27×10^{-2} K s^{-1}. In each cycle, reverse martensitic transformation ended with a higher absolute rate than it started.

The following variation tendencies were noted, while increasing both the heating temperature and the number of cycles: (i) the process was shifted to lower temperatures and became less intense, up to total extinction; (ii) the entire process became slower in such a way that the absolute values of the transformation rates decreased more than 12 times for the beginning and almost four times at the end of martensite reversion; and (iii) the gradual loss of thermal memory was ascribed to the formation of lath-martensite under the form of stabilized interlocking needles.

Acknowledgment

This study was financially supported by UEFISCU by means of the research grant PN II-ID 301-PCE-2007-1, contract no. 279/01.10.2007

References

1. C.M. Wayman and T.W. Duerig, An Introduction to Martensite and Shape Memory, *Engineering Aspects of Shape Memory Alloys*, T.W. Duerig, K.N. Melton, D. Stöckel, and C.M. Wayman, Ed., Butterworth-Heinemann, Oxford, 1990, p 3–20
2. T. Tadaki, Cu-Based Shape Memory Alloys, *Shape Memory Materials*, K. Otsuka and C.M. Wayman, Ed., Cambridge University Press, Cambridge, 1998, p 97–116
3. P.K. Kumar and D.C. Lagoudas, Introduction to Shape Memory Alloys, *Shape Memory Alloy Modelling and Engineering Applications*, D.C. Lagoudas, Ed., Springer, New York, 2008, p 1–51
4. T.W. Duerig, K.N. Melton, and J.L. Proft, Wide Hysteresis Shape Memory Alloys, *Engineering Aspects of Shape Memory Alloys*, T.W. Duerig, K.N. Melton, D. Stöckel, and C.M. Wayman, Ed., Butterworth-Heinemann, Oxford, 1990, p 130–136
5. P. Tautzenberger, Thermal Actuators: A Comparison of Shape Memory Alloys with Thermostatic Bimetals and Wax Actuators, *Engineering Aspects of Shape Memory Alloys*, K.N. Melton, D. Stöckel, and C.M. Wayman, Ed., Butterworth-Heinemann, Oxford, 1990, p 207–218
6. Pre-Tensioned Shape Memory Actuator, U.S. Patent 4,899,543, http://www.patentvest.com/console/reports/docs/grant/04899543.html
7. W. Van Moorleghem and D. Otte, The Use of Shape Memory Alloys for Fire Protection, *Engineering Aspects of Shape Memory Alloys*, K.N. Melton, D. Stöckel, and C.M. Wayman, Ed., Butterworth-Heinemann, Oxford, 1990, p 295–302
8. E. Weynant and G. Barreau, Nouvelles Applicctions industrielles d'alliages à mémoire de forme (Cu-Zn-Al), *Trait. Therm.*, 1990, **234**, p 57–62
9. L.G. Bujoreanu, S. Stanciu, A. Enache, C. Lohan, and I. Rusu, Influence of Some Extrinsic Factors on the Two Way Shape Memory Effect of Electric Actuators, *J. Optoelectron. Adv. Mater.*, 2008, **10**(3), p 602–606
10. R. Kainuma, J.J. Wang, T. Omori, Y. Sutou, and K. Ishida, Invar-type Effect Induced by Cold-Rolling Deformation in Shape Memory Alloys, *Appl. Phys. Lett*, 2002, **80**, p 4348–4350
11. L. Delaey and J. Smeesters, Discussion to Paper 31, *Shape Memory Effects in Alloys*, J. Perkins, Ed., Plenum Press, New York, 1975, p 577–578
12. J.M. Guilemany, J. Fernandez, R. Franch, A.V. Benedetti, and A.T. Adorno, A New Cu-Based SMA With Extremely High Martensitic-Transformation Temperatures, *J. Phys. IV*, 1995, **C2**, p 361–365
13. N. Si, K. Sun, S. Sun, and H. Liu, Damping Performance of Cu-Zn-Al Shape Memory Alloys in Engineering Structures, *J. Cent. South Univ. Technol.*, 2004, **11**, p 246–251
14. L. Manosa, A. Planes, E. Vives, and R. Romero, The Use of Shape-Memory Alloys for Mechanical Refrigeration, *Funct. Mater. Lett.*, 2009, **2**(2), p 73–78
15. I. Ohkata and Y. Suzuki, The Design of Shape Memory Alloys Actuators and Their Applications, *Shape Memory Materials*, K. Otsuka and C.M. Wayman, Ed., Cambridge University Press, Cambridge, 1998, p 240–266
16. R.F. Gordon, Design Principles for Cu-Zn-Al Actuators, *Engineering Aspects of Shape Memory Alloys*, T.W. Duerig, K.N. Melton, D. Stöckel, and C.M. Wayman, Ed., Butterworth-Heinemann, Oxford, 1990, p 245–255
17. J. Cederstrom, V. Kolomytsev, A. Kozlov, P. Titov, G. Zatulskii, and S. Kondratjuk, Evolution of the Shape Memory Parameters During Multiple Transformation Cycles Under Load in Cu-Zn-Al Alloys, *Mater. Sci. Eng. A*, 1999, **273–275**, p 804–808
18. A. Yawny, M. Sade, and F.C. Lovey, Conceptual Design of Actuator Applications with Cu-Zn-Al Single Crystals, *Mater. Sci. Eng. A*, 1999, **273–275**, p 789–794
19. V. Sampath, Effect of Thermal Processing on Microstructure and Shape-Memory Characteristics of a Copper-Zinc-Aluminum Shape Memory Alloy, *Mater. Manuf. Process.*, 2007, **22**, p 9–14
20. M. Franz and E. Hornbogen, Martensitic Transformation of a CuZnAl-Shape Memory Alloy Strengthened by Hot-Rolling, *Mater. Sci. Eng. A*, 1999, **252**, p 157–165
21. F.C. Lovey and V. Torra, Shape Memory in Cu-Based Alloys: Phenomenological Behavior at the Mesocale Level and Interaction of Martensitic Transformation with Structural Defects in Cu-Zn-Al, *Prog. Mater. Sci.*, 1999, **44**, p 189–289
22. M. Sade, C. Damiani, R. Gastien, F.C. Lovey, J. Malaria, and A. Yawni, Fatigue and Martensitic Transitions in Cu-Zn-Al and Cu-Al-Ni Single Crystals: Mechanical Behaviour, Defects and Diffusive Phenomena, *Smart Mater. Struct.*, 2007, **16**, p S126–S136
23. L.G. Bujoreanu, M.L. Craus, I. Rusu, S. Stanciu, and D. Sutiman, On the β2 to α Phase Transformation in a Cu-Zn-Al—Based Shape Memory Alloy, *J. Alloys Compd.*, 1998, **278**, p 190–193
24. L.G. Bujoreanu, M.L. Craus, S. Stanciu, and V. Dia, Thermally and Stress Induced Changes in Three Phase Structure of Cu-Zn-Al-Fe Shape Memory Alloy, *Mater. Sci. Technol.*, 2000, **16**, p 612–616
25. L.G. Bujoreanu, On the Influence of Austenitization on the Morphology of α-Phase in Tempered Cu-Zn-Al Shape Memory Alloys, *Mater. Sci. Eng. A*, 2008, **481–482**, p 395–403
26. A.K. Bhuniya, P.P. Chattopadhyay, S. Datta, and M.K. Banerjee, On the Degradation of Shape Memory Effect in Trace Ti-Added Cu-Zn-Al Alloy, *Mater. Sci. Eng. A*, 2005, **393**, p 125–132
27. F.J. Gil and J.M. Guilemany, The Determination of the Electron to Atom Ratio Interval Corresponding to the Change in the Martensitic Structure from α′ to β′ in Cu-Zn-Al Shape Memory Alloys, *Mater. Res. Bull.*, 1992, **27**, p 117–122
28. V. Dia, L.G. Bujoreanu, S. Stanciu, and C. Munteanu, Study of the Shape Memory Effect in Lamellar Helical Springs Made from Cu-Zn-Al Shape Memory Alloy, *Mater. Sci. Eng. A*, 2008, **481–482**, p 697–701
29. J. Spielfield, Marforming and Martempering of a Cu-Zn-Al Shape Memory Alloy, *Mater. Sci. Eng. A*, 1999, **273–275**, p 639–643
30. V.J. Griffin and P.G. Laye, Differential Thermal Analysis and Differential Scanning Calorimetry, *Thermal Analysis—Techniques and Applications*, E.L. Charsley and S.B. Warrington, Ed., Royal Society of Chemistry, Cambridge, 1992, p 17–30
31. M. Benke, F. Tranta, P. Barkoczy, V. Mertinger, and L. Daroczi, Effects of Heat-Flux Features on the Differential Scanning Calorimetry Curve of a Thermoelastic Martensitic Transformation, *Mater. Sci. Eng. A*, 2008, **481–482**, p 522–525
32. J.L. Pelegrina and V. Torra, Comment on "Effects of Heat-Flux Features on the Differential Scanning Calorimetry Curve of a Thermoelastic Martensitic Transformation" by Benke et al. [Mater. Sci. Eng. A 481–482 (2008) 522]. *Mater. Sci. Eng. A*., 2009. doi: 10.1016/j.msea.2009.06.053
33. W-J Zhu, W-Y Chen, and T.Y. Hsu (Xu Zuyao), Group Theory and Crystallography of the Martensitic Transformation in a Cu-26.71Zn-4.15Al Shape Memory Alloy, *Acta Metall.*, 1985, **33**, p 2075–2082
34. J. Van Humbeeck, Aspects microstructuraux: relations entre la transformation martensitique et les propriétés thermomécaniques, *Technologie des Alliages à Mémoire de Forme*, E. Patoor and M. Berveiller, Ed., Hermès, Paris, 1994, p 89–113
35. T. Saburi, C.M. Wayman, K. Takata, and S. Nenno, The Shape Memory Mechanism in 18R Martensitic Alloys, *Acta Metall.*, 1980, **28**, p 15–23
36. E.-S. Lee and Y.G. Kim, A Transformation Kinetic Model and Its Application to a Cu-Zn-Al Shape Memory Alloy. I. Isothermal Conditions, *Acta Metall. Mater.*, 1990, **38**, p 1669–1676
37. L.G. Bujoreanu, S. Stanciu, P. Barsanescu, and N.M. Lohan, Study of the Transitory Formation of α_1 Bainite, as a Precursor of α-Phase in Tempered SMAs, *Advanced Topics in Optoelectronics, Microelectronics and Nanotechnologies IV.*, P. Schiopu, C. Panait, G. Caruntu, and A. Manea, Ed., Proc. SPIE Vol 7297, 72970B1-6